Earth and Planetary Science Letters 500 (2018) 205–214

Contents lists available at ScienceDirect

Earth and Planetary Science Letters

www.elsevier.com/locate/epsl

Early loss, fractionation, and redistribution of chlorine in the Moon as revealed by the low-Ti lunar mare basalt suite

Jeremy W. Boyce [a,*], Sarah A. Kanee [a], Francis M. McCubbin [a], Jessica J. Barnes [a], Hayley Bricker [b], Allan H. Treiman [c]

[a] NASA – Johnson Space Center, 2101 NASA Parkway, Houston, TX 77058, United States of America
[b] Department of Physics and Astronomy, UCLA, 475 Portola Plaza, Los Angeles, CA, 90095-1547, United States of America
[c] Lunar and Planetary Institute, 3600 Bay Area Boulevard, Houston, TX 77058, United States of America

ARTICLE INFO

Article history:
Received 28 March 2018
Received in revised form 26 July 2018
Accepted 30 July 2018
Available online 23 August 2018
Editor: F. Moynier

Keywords:
Moon
lunar
volatiles
non-traditional stable isotopes
formation
modeling

ABSTRACT

The relative abundances of chlorine isotopes measured in low-Ti basalts from the Moon appear to reflect mixing between two reservoirs: One component representing the urKREEP—the final product of the crystallization of the lunar magma ocean—with $\delta^{37}Cl = +25‰$ (relative to Standard Mean Ocean Chlorine), the other representing either a mare basalt reservoir or meteoritic materials with $\delta^{37}Cl \sim 0‰$. Using the abundances of other KREEP-enriched elements as proxies for the abundance of Cl in low-Ti mare basalts—which is difficult to constrain due to magmatic processes such as fractional crystallization and degassing—we find that the urKREEP contains ~28 times higher Cl abundance (25–170 ppm Cl) as compared to the low-$\delta^{37}Cl$ end member in the observed mixing relationship. Chlorine—with an urKREEP/C.I. ratio of 0.2 to 1.5—is 500 to 3400 times less enriched than refractory incompatibles such as U and Th, and is consistent with incomplete loss of Cl species taking place during or prior to the magma ocean phase. The preservation of multiple, isotopically distinct reservoirs of Cl can be explained by: 1) Incomplete degassing pre- or syn-giant impact, with preservation of undegassed chondritic Cl and subsequent formation of an enriched and isotopically fractionated reservoir; or 2) Development of both high-concentration, high-$\delta^{37}Cl$ and low-concentration, low-$\delta^{37}Cl$ reservoirs during the degassing and crystallization of the lunar magma ocean. A range of model bulk lunar Cl abundances from 0.3–0.6 ppm allows us to place Cl in the context of the rest of the elements of the periodic table, and suggests that Cl behaves as only a moderately volatile element during degassing. Chlorine isotope fractionation resulting from loss syn- or pre-magma ocean is characterized by $1000 \bullet \ln[\alpha] = -3.96$ to -4.04. Abundance and isotopic constraints are consistent with the loss of Cl being limited by vaporization of mixtures of Cl salts such as HCl, $ZnCl_2$, $FeCl_2$, and NaCl. These new constraints on the chlorine abundance and isotopic values of urKREEP make it a well-constrained target for dynamic models aiming to test plausible conditions for the formation of the Earth–Moon system.

1. Introduction

The systematic depletion of volatile elements in lunar rocks and estimates of bulk lunar abundances based on those rocks is a fundamental constraint on the formation and evolution of the Earth–Moon system (Barr, 2016 and references therein; Day and Moynier, 2014; Hauri et al., 2015; McCubbin et al., 2015a). The loss of moderately to highly volatile elements is also associated with measurable—in some cases quite large—isotopic fractionations (Day and Moynier, 2014; Day et al., 2017; Herzog et al., 2009; Kato and Moynier, 2017; Paniello et al., 2012; Pringle and Moynier, 2017; Wang and Jacobsen, 2016a). One such example is Cl, which has two stable isotopes (^{35}Cl and ^{37}Cl) that are fractionated tens of per mille (‰; parts per thousand) more in lunar rocks than in their terrestrial equivalents (Sharp et al., 2010a). There are two kinds of chlorine isotope data available for lunar basalts: 1) High-precision ($<1‰$ 2σ) conventional mass spectrometry measurements, sometimes reported with separate $\delta^{37}Cl$ measurements on soluble and insoluble portions of bulk samples, and 2) Lower-precision (1–3‰ 2σ), *in situ* secondary ion mass spectrometry (SIMS) measurements of the Cl-rich phase apatite, a mineral that

* Corresponding author.
E-mail address: jwboyce@alum.mit.edu (J.W. Boyce).

https://doi.org/10.1016/j.epsl.2018.07.042

is present in most lunar basalts. For variations of the magnitude observed on the Moon (from −4‰ to +81‰; Boyce et al., 2015; Wang et al., 2012), both techniques can provide useful but different information about the rocks sampled.

Early models (Sharp et al., 2010a) based on a combination of SIMS and conventional mass spectrometry data suggested that these highly fractionated basalts could only form by anhydrous degassing of metal chloride such as NaCl, $FeCl_2$, or $ZnCl_2$ during eruption. However, this model is inconsistent with experimental data showing large fractionations during evaporation of HCl (Sharp et al., 2010b), the presence of hydrogen in samples with elevated δ^{37}Cl (Boyce et al., 2010, 2015; Greenwood et al., 2011; McCubbin et al., 2010; Potts et al., 2018), and the observation that the highest Cl abundances are associated with elevated δ^{37}Cl (Barnes et al., 2016; Boyce et al., 2015).

An alternative model was presented by Boyce et al. (2015) and later by Barnes et al. (2016) in which elevated δ^{37}Cl measurements were attributed to mixing between light and heavy isotopic reservoirs of Cl within the Moon: The light reservoir ($\delta^{37}\text{Cl} \leq 0$‰) was suggested to be the uncontaminated signal of mare basalts, whereas the heavy reservoir ($\delta^{37}\text{Cl} > +25$‰) was attributed to the urKREEP—the last vestige of the lunar magma ocean. The fractionation mechanisms proposed by Sharp et al. (2010a) are consistent with the model of Boyce et al. (2015) with the caveat that the timing of degassing was different with the latter model attributing the degassing and related fractionation to the magma ocean following the giant impact that formed the Earth–Moon system. Incompatible elements—including Cl—are assumed to be concentrated into the urKREEP during the crystallization of the lunar magma ocean (Warren and Wasson, 1978, 1979). Correlations between these abundances and δ^{37}Cl are the primary evidence for the urKREEP being the source of heavy Cl on the Moon (Boyce et al., 2015).

Here, we continue this line of thinking to use chlorine isotopes in lunar basalts to further constrain the planet-scale chemical evolution of the early Earth–Moon system.

1.1. Relationship between chlorine isotopes and incompatible elements

Elevated δ^{37}Cl values are observed in apatite crystals that are rich in Cl, consistent with a reservoir enriched in Cl, and relatively enriched in ^{37}Cl over ^{35}Cl (Boyce et al., 2015). Chlorine isotope ratios are also observed to increase with increasing bulk Th and La/Lu, both indicators of an urKREEP component in the basalt (Neal and Taylor, 1989; Warren and Wasson, 1978). Barnes et al. (2017) noted that this relationship only appears to hold for low-Ti and KREEP-rich basalts (which are also low in Ti), but that high-Ti basalts do not appear to define the same δ^{37}Cl-trace element relationship. This is consistent with overall petrogenetic relationships of the low-Ti and high-Ti basalts, which are thought to derive from different source regions within the lunar mantle, possibly at different depths (Krawczynski and Grove, 2012; Longhi, 1992; Shearer et al., 2006). It is also consistent with the "neuKREEP" hypothesis of Jerde and Taylor (Jerde et al., 1993; Jerde and Taylor, 1993), who suggested that the high-Ti basalts derived their trace element systematics by incorporating a different material than did the low-Ti basalts. The recent work of Barnes et al. (2017) supports this hypothesis, although more work is needed to determine and subsequently evaluate the systematics of the high-Ti basalts, which are not described in detail here.

In order to test the hypothesis that the urKREEP is the source of elevated δ^{37}Cl in low-Ti and KREEP basalts, we have expanded the analysis of Boyce et al. (2015) comparing in situ δ^{37}Cl measured in apatite and bulk trace elements to include a larger number of samples. When considering any δ^{37}Cl-trace element relationship, one concern is that the elements correlating positively with δ^{37}Cl are all compatible in apatite (Cl, Th, REE), which might implicate apatite itself as the culprit in generating these relationships. One possibility would be that there is an unidentified lithology with ^{37}Cl-rich, Cl-rich apatites that can generate mixing arrays via contamination. In order to address this we have also considered a wider range of elements with different geochemical affinities including large ion lithophile (K, Ba) and high field strength (Zr, Hf) elements, which do not partition favorably into apatite. This choice of elements with diverse geochemical behavior—saving for their incompatibility in the phases crystallizing from the lunar magma ocean—uniquely tests the hypothesis that the urKREEP is the source of elevated δ^{37}Cl in the low-Ti suite of lunar mare basalts.

1.2. Mixing models

Ideally, one would use hyperbolic mixing relationships to constrain the isotopic composition of the two end members (in this case $\delta^{37}\text{Cl}_{\text{mare}}$ and $\delta^{37}\text{Cl}_{\text{urKREEP}}$), as well as the elemental abundances (Cl_{mare} and $\text{Cl}_{\text{urKREEP}}$, with the former representing the KREEP-free abundance in mare basalts, and the latter representing the Cl content of the urKREEP). This would be a valuable contribution to our understanding of the Moon, as Cl is a volatile element and the volatile budget of the Moon is an important and active field of study (Hauri et al., 2015). However, the aforementioned analysis requires knowledge of the Cl content of the basalts studied. This is a problem because the three methods we have for constraining the Cl content of mare basalts—bulk measurements; melt inclusions; apatite volatile barometry—are flawed (see supplemental information). The almost certainty with which the assertions of any $\delta^{37}\text{Cl}$–$\text{Cl}_{\text{apatite}}$ model that relies on Cl estimates are violated would make any result suspect at best. In the following paragraphs we outline a more robust strategy.

1.3. Modeling Cl isotopic mixing by proxy

The concomitant enrichment of all incompatible elements in the urKREEP provides an alternative to using Cl abundances in bulk rocks or apatites to constrain Cl_{mare} and $\text{Cl}_{\text{urKREEP}}$. We can use other elements for which more robust bulk estimates are available as proxies for Cl, and build mixing models with those elements taking the place of Cl. For mixtures with component moles of Cl here labeled Cl_A, Cl_B, (etc.), and isotopic compositions $\delta^{37}\text{Cl}_\text{A}$, $\delta^{37}\text{Cl}_\text{B}$, (etc.), the canonical equation for mixtures where the components have small differences is given by

$$\delta^{37}\text{Cl}_{\text{Total}}\text{Cl}_{\text{Total}} \approx \delta^{37}\text{Cl}_\text{A}\text{Cl}_\text{A} + \delta^{37}\text{Cl}_\text{B}\text{Cl}_\text{B} + \delta^{37}\text{Cl}_\text{C}\text{Cl}_\text{C} + \cdots \quad (1)$$

this simplifies in the binary case to solve for a magma contaminated by urKREEP to be:

$$\delta^{37}\text{Cl}_{\text{Total}} \approx \frac{(\delta^{37}\text{Cl}_{\text{mare}}\text{Cl}_{\text{mare}} + \delta^{37}\text{Cl}_{\text{urKREEP}}\text{Cl}_{\text{urKREEP}})}{\text{Cl}_{\text{Total}}} \quad (2)$$

It should be noted that the approximation used above differs slightly from the exact solution—which treats moles of ^{35}Cl and ^{37}Cl as separate species instead of relying on δ^{37}Cl values—by ≤0.04‰ for these scenarios. In our case, Cl_{mare} and $\text{Cl}_{\text{urKREEP}}$ in Eq. (2) are unknown. We can use other elements for which more robust bulk estimates are available as proxies for Cl, and build mixing models with those elements taking the place of Cl:

$$\delta^{37}\text{Cl}_{\text{Total}} \approx \frac{(\delta^{37}\text{Cl}_{\text{mare}}\text{X}_{\text{mare}} + \delta^{37}\text{Cl}_{\text{urKREEP}}\text{X}_{\text{urKREEP}})}{\text{X}_{\text{Total}}} \quad (3)$$

where X no longer represents chlorine, but rather a proxy element (K, U, La, Hf, etc.) where X $\propto$ Cl. Models constructed with proxies can constrain the isotopic composition of the two end members. However, because the ratios of the abundance of Cl to the abundances of various proxy elements (Cl/La, Cl/K, Cl/U, etc.) are not known *a priori* for any sample, we cannot use these models to determine the absolute concentrations (Cl_{mare} and $Cl_{urKREEP}$) in the two end members. Simple numerical experiments—varying the input mare basalt abundance and watching the resulting model results—confirm that we are limited to constraining the "enrichment factor", which is the ratio of the two end member Cl abundances ($Cl_{urKREEP}/Cl_{mare}$). This reduces the model to one with only three variables: The isotopic composition of the two end members ($\delta^{37}Cl_{mare}$ and $\delta^{37}Cl_{urKREEP}$), and the enrichment factor. We use a geochemically diverse suite of elements as proxies for Cl: K, Ba, La, Lu, Th, U, Zr, and Hf. All of these elements are incompatible and enriched in urKREEP by a factor of ~14 (K) to ~750 (Th and U) over the abundances of the same elements in CI chondrite (Neal and Taylor, 1989; Warren, 1989; Warren and Wasson, 1979).

1.4. Model space search approach

In a traditional mixing model, one would best fit data in $\delta^{37}Cl$ versus Cl_{mare} model space. One could invert the data and solve directly for the solution in a least squares sense, or by varying the parameters until a best fit is achieved (a forward modeling approach). The modeling described here is a form of the latter, with a set of trace elements serving as proxies for Cl abundance. In order to find the single set of $\delta^{37}Cl_{urKREEP}$, $\delta^{37}Cl_{mare}$, and $Cl_{urKREEP}/Cl_{mare}$ parameters that best fits all eight elements modeled here, we use a brute-force model space search forward modeling technique, similar to, but less elegant than, methods commonly applied to solve inverse problems in seismology (Beghein, 2010; Xing and Beghein, 2015). For any or all of the proxy elements, we calculate a mixing curve for each set of abundance and isotope parameters, then use this curve to calculate the misfit to the data (in the $\delta^{37}Cl$ dimension). This process is repeated for a wide range of values, establishing which set of mixing parameters yields the best fit to the data. We fit all eight proxy elements simultaneously (in addition to individually) because the ability to fit different proxies with a single set of parameters is a critical test of the assumption of the model—first and foremost that two-component mixing is taking place, and that it is responsible for the variations observed—and second of all, that the urKREEP is one of the end members.

Forward modeling not only allows us to determine the best fit set of parameters, but also allows us to determine (at least in a relative sense) the uncertainty on each parameter, as we can observe how the misfit changes as we change the values in the model. Model-space search approaches also reveal tradeoffs between parameters: different parameters that can have the same effect on the goodness of fit of the model as other parameters. A further shortcoming of proxy modeling is that we are unable to discriminate between some different scenarios that have similar $Cl_{urKREEP}/Cl_{mare}$ ratios, which prevents us from determining the absolute abundance of Cl in the two end members without additional, outside constraints. However, these constraints exist and are discussed in detail below.

Models were run for scenarios encompassing all low-Ti basalts as well as KREEP-basalts that are also low in Ti (Fig. 1). High-Ti basalts are excluded on the grounds that they are genetically different—derived from a different part of the mantle with different major, minor, and trace element characteristics. A similar argument about magmatic source and trace element characteristics can be made for VHK basalts, so data from VHK basalt 14304 is discarded despite it adhering well to the model. The $\delta^{37}Cl$ values of the Mg-suite rocks are consistent with an urKREEP origin

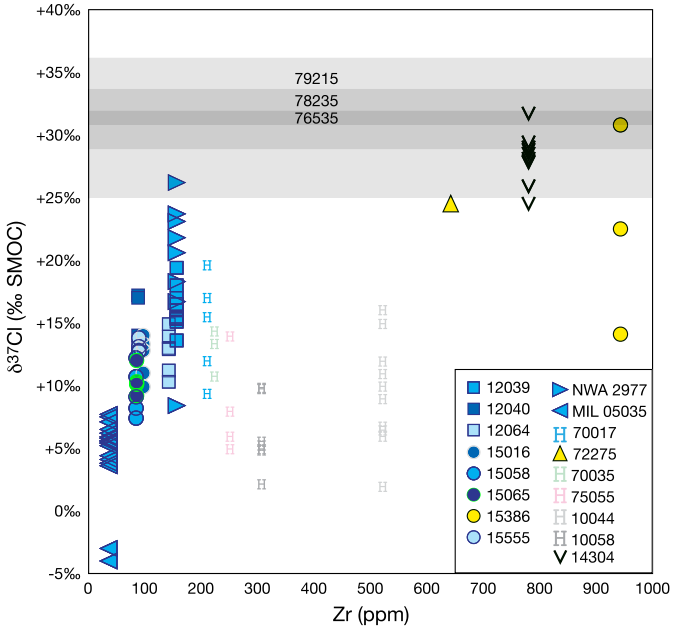

Fig. 1. $\delta^{37}Cl$ measurements in apatite available in the literature—excluding breccias, which do not have meaningful elemental abundances in the context of a mixing model, because they themselves are mixtures of many components—plotted as a function of Zr content (see main text for references). Low-Ti basalts are plotted as blue symbols, whereas the KREEP-rich low-Ti basalts called "KREEP-basalts" are yellow. High-Ti basalts (Barnes et al., 2017; Boyce et al., 2015) are plotted as the letter "H", whereas the VHK basalt 14304 is plotted as the letter "V". Intrusives are plotted as grey bands, consistent with their association with the urKREEP (Barnes et al., 2016) and cumulate nature (making trace element abundances uninterpretable in the context of this model). Only low-Ti basalts (blue) and low-Ti KREEP basalts (yellow) are modeled in this manuscript, consistent with previous thinking on the origin of trace element signatures in the low-Ti basalt suite (which includes the KREEP basalts). (For interpretation of the colors in the figure(s), the reader is referred to the web version of this article.)

(Barnes et al., 2016; McCubbin et al., 2015a), but their trace element abundances are not comparable to the basalts because of their cumulate nature, so they are not included in our modeling efforts. Nonetheless, the $\delta^{37}Cl$ values of the Mg-suite samples offer an important point of comparison when trying to interpret the model results (Fig. 1).

2. Data

Chlorine isotope data for the model come from a number of sources in the literature. Apollo 12 low-Ti basalts 12039 and 12040 were studied by Boyce et al. (2015), Sharp et al. (2010a), whereas the data for 12064 is reported in Barnes et al. (2018) along with additional data for 12039. Apollo 14 VHK basalt 14304 was analyzed by Barnes et al. (2016), as were Apollo 15 low-Ti (15555) and KREEP (15386) basalts, as well as high-Ti basalts 10044, 10058, and 70035. Data for low-Ti basalts 15016, 15058, 15065 and 70017 are from Barnes et al. (2018), as is data for meteorite MIL 05035. Chlorine isotope data for KREEP basalt 72275 comes from Sharp et al. (2010a). Data for low-Ti basalts from meteorites MIL 05035 and NWA 2977 were reported in Wang et al. (2012) and Boyce et al. (2015), the latter providing data for high-Ti basalt 75055 as well. For each sample, all available measurements were averaged on a thin-section by thin-section basis, the argument being that different sections might represent natural variability in $\delta^{37}Cl$, but that studies with greater numbers of analyses on a particular section shouldn't be permitted to skew the model results. Trace element data comes from the Lunar Sample Compendium (Meyer, 2009) as well as Joy et al. (2008), Liu et al. (2009), and Hallis et al. (2014), and is a compilation of measurements of a wide range

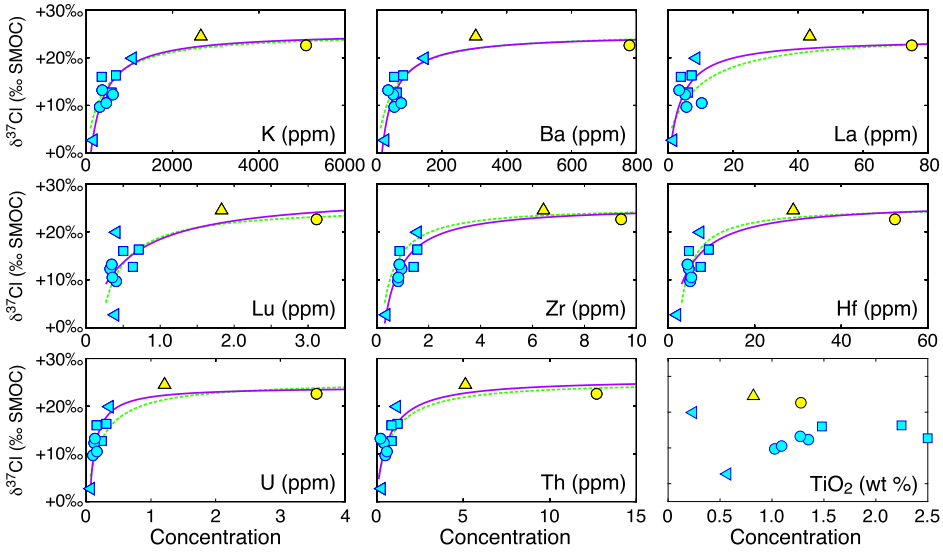

Fig. 2. δ^{37}Cl plotted as a function of KREEPy elements K, Ba, La, Lu, Zr, Hf, U, and Th. For each symbol, the chlorine isotope value is the mean of published measurements of δ^{37}Cl in apatite (Barnes et al., 2008; Boyce et al., 2015; McCubbin et al., 2012; Sharp et al., 2010a), whereas elemental abundance is the mean of individual element values from the Lunar sample compendium (Meyer, 2009) as well as Joy et al. (2008), Liu et al. (2009), and Hallis et al. (2014). Simultaneous best fit curve for all elements shown in green dashed line, best fit curve for individual element shown in purple. KREEP (yellow), and other low-Ti (cyan) basalts plotted with symbols differentiating samples from Apollo 12 (squares), 15 (circles), and 17 (upward triangles) suites, as well as meteorites (left triangles), where sample names are the same as in Fig. 1. Last panel plots δ^{37}Cl versus TiO_2 to demonstrate that KREEP-basalts are part of the suite of low-Ti basalts.

Table 1
Input and output parameters for the models described in the text. Simultaneous fit of all elements yields a best fit $\delta^{37}Cl_{urKREEP} = +24.4‰$, $\delta^{37}Cl_{mare} = +5‰$, and $Cl_{urKREEP/mare} = 23$, whereas the mean of the individual element fits (weighted by the sum of the square of the misfits for each datum) yields $\delta^{37}Cl_{urKREEP} = +24.5‰$, $\delta^{37}Cl_{mare} = +3‰$, and $Cl_{urKREEP/mare} = 28$.

Input parameters			Best fit parameters		
Elements	Mare (ppm)	urKREEP (ppm)	[Cl]urKREEP/mare	$\delta^{37}Cl_{mare}$	$\delta^{37}Cl_{urKREEP}$
K	97	10700	33	−0.7‰	24.6‰
Ba	12	1300	38	−2.9‰	24.2‰
La	1.1	230	53	2.6‰	23.6‰
Lu	0.26	7.8	11	9.1‰	26.3‰
Zr	31	1400	21	0.9‰	24.3‰
Hf	1.6	38	11	9.1‰	24.7‰
U	0.06	6.1	61	2.1‰	23.7‰
Th	0.12	22	27	4.7‰	25‰
Weighted mean of individual elements*			28	3 ± 9‰ 2s	24.5 ± 1.7‰ 2s
All elements simultaneously			23	5‰	24.4‰

of elements, made by different techniques, with commensurately different levels of reliability. For the trace elements we use the arithmetic mean of available data to characterize each sample.

3. Results

For all the proxy elements studied (K, Ba, La, Lu, Zr, Hf, U, Th), plots of δ^{37}Cl versus proxies show positive, strongly non-linear correlations consistent with two-component mixing between a reservoir with elevated $^{37}Cl/^{35}Cl$ and elevated abundances of all proxy elements and a second reservoir with low $^{37}Cl/^{35}Cl$ and low trace element abundances (Fig. 2). Best fit δ^{37}Cl and Cl_{mare} and $Cl_{urKREEP}$ abundances are given in Table 1. For single-proxy element models (purple curves on Fig. 2), best fit $\delta^{37}Cl_{mare}$ values range from −3‰ to +9‰, with a weighted arithmetic mean of −3‰ ± 9‰. Best fit $\delta^{37}Cl_{urKREEP}$ values range between +23.6‰ and +26.3‰, with a mean of +24.5‰ ± 1.7‰. Ratios of $Cl_{urKREEP}/Cl_{mare}$ range from 11 to 61 with a weighted logarithmic mean of 28. The best constraint is for $\delta^{37}Cl_{urKREEP}$, which is unsurprising given that the high-δ^{37}Cl limb of the mixing hyperbole is well constrained by several KREEP basalts. Furthermore, the $\delta^{37}Cl_{urKREEP}$ is similar to the Cl isotopic composition of the Mg-suite samples (gray bars in Fig. 1) that were reported, based on their petrogenetic histories (e.g., Shearer et al., 2015), to represent the Cl-isotopic composition of urKREEP (Barnes et al., 2016; McCubbin et al., 2015a). In contrast, the low-δ^{37}Cl limb is pinned almost entirely by one sample, MIL 05035, and all of the samples with δ^{37}Cl also have low trace element abundances, making measurements generally less certain. Despite the scatter, every model yields $\delta^{37}Cl_{mare}$ values that are distinctly lower than the commensurate $\delta^{37}Cl_{urKREEP}$.

Fitting all the proxy elements simultaneously yields a single set of best fit parameters (green curves in Fig. 2) with $\delta^{37}Cl_{mare} = +5‰$, $\delta^{37}Cl_{urKREEP} = +24.4‰$, and $Cl_{urKREEP}/Cl_{mare} = 23$. These values are similar to the means derived from individual fits, though with higher $\delta^{37}Cl_{mare}$ and lower $Cl_{urKREEP}/Cl_{mare}$. The difference between the two lies in how the fitting was done: The mean of individual fits is weighted by the misfit of each δ^{37}Cl-proxy model. In contrast, the simultaneous fit is uniformly weighted across all elements. Because it takes into account all the data and provides a robust estimate of uncertainty, we declare the mean of the individual best fits to be our preferred values for the outcome of the model. All of the discussion to follow this section is based upon this set of parameters. The simultaneous fit does satisfy the test

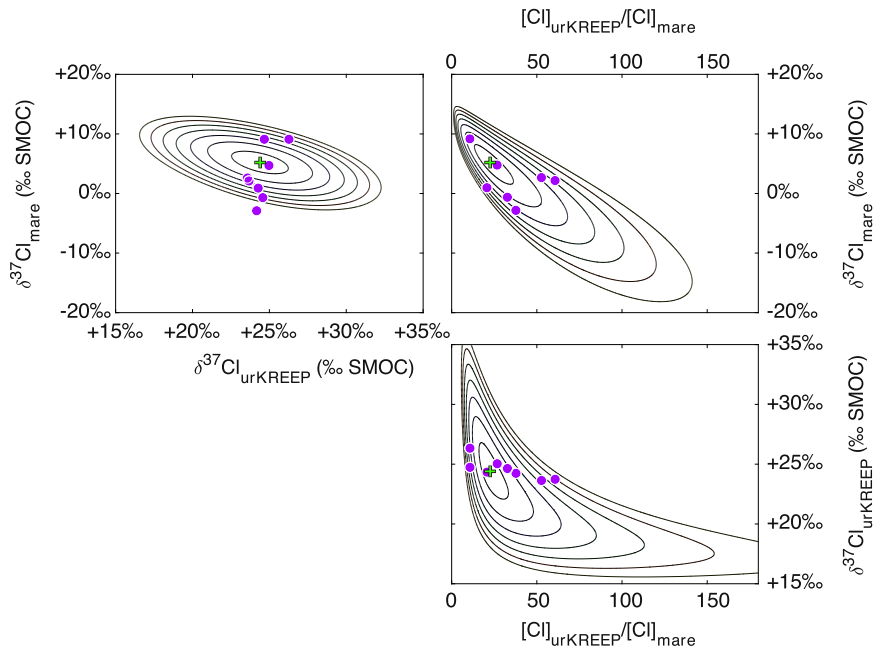

Fig. 3. Goodness of fit maps for $\delta^{37}Cl_{mare}$, $\delta^{37}Cl_{urKREEP}$, and $Cl_{urKREEP}/Cl_{mare}$ for all data fit simultaneously. Contours represent areas (sets of model parameters) that yield similar misfits to the data and are therefore impossible to distinguish based on misfit. The best fit set of parameters (green cross) has a mean average deviation (MAD) = 1.4‰, whereas the edge of outermost region represents MAD = 2‰. Purple symbols indicate best fit parameters (equivalent of green cross) for individual elements. Note the strong correlations between the enrichment factor ($Cl_{urKREEP}/Cl_{mare}$) and the $\delta^{37}Cl$ of the model end members.

of fitting all the data with a single set of parameters (Fig. 2): The extent to which all of the geochemically diverse incompatible elements can be well-fit by a single set of fitting parameters suggests a high degree of internal consistency both in the assertions of the mixing model and the end member abundances of the proxies. Using different trace element abundances for the urKREEP end-member makes only subtle differences in the goodness of fit of the models, and in the best fit values. For example, choosing lower La (110 ppm instead of 233) and higher Zr (1700 ppm instead of 1400) and other values as suggested by Warren and Wasson (1979) results in best fit model parameters of $\delta^{37}Cl_{mare} = +4‰$, $\delta^{37}Cl_{urKREEP} = +24.1‰$, and $Cl_{urKREEP}/Cl_{mare} = 21$, nearly indistinguishable from the simultaneous fit with the preferred values.

Absolute uncertainty estimates are derived from statistics on the individual element model fits, except for the ratio of the abundances of Cl in urKREEP and Cl in the mare basalt, which as a bounded function (in this case by zero, as negative ratios are not permitted) would yield an average and standard deviation that are not representative of the data. Modeling the ratios as a bounded function such as a lognormal distribution leads to a mean and uncertainty estimate of 28^{+57}_{-19}, which agrees with the arithmetic mean and emphasizes the preference of the model for higher ratios. In addition to this conventional approach to error estimation, the forward modeling approach employed here allows us to generate "topographic" maps of misfit (Fig. 3), which clearly demonstrate the model space regions with approximately equally "good" model fits. A forward model approach to solving this problem also allows us to see the relationships (or "trade-offs") between different parameters. For example, we see that there are expected trade-offs between the enrichment factor and the two end-member isotopic compositions ($\delta^{37}Cl_{urKREEP}$ and $\delta^{37}Cl_{mare}$). It is important to note that the distribution of best fit values on the $Cl_{urKREEP}/Cl_{mare}$ ratio is highly asymmetric (Fig. 3), typical of bounded functions. The data are significantly more permissive of higher enrichment factors than with lower ratios: Models with 8–59 times more Cl in urKREEP than in the low-$\delta^{37}Cl$ end member fit the data at least twice as well (half the misfit) as models with equal amounts of Cl in both end members. In other words, Cl enrichment is strongly favored over Cl parity.

4. Discussion

4.1. Implications of multiple Cl reservoirs

The most fundamental result of the modeling is that a single set of $\delta^{37}Cl_{urKREEP}$, $\delta^{37}Cl_{mare}$, and $Cl_{urKREEP}/Cl_{mare}$ fits all of the "KREEPy" proxy element-$\delta^{37}Cl$ relationships (Fig. 2) for both KREEP-rich and KREEP-poor low-Ti basalts. This is consistent with the presence of two distinct reservoirs, and supports the hypothesis that the urKREEP is a source of high-$\delta^{37}Cl$ chlorine in at least some mare basalts. The mere existence of multiple reservoirs of isotopically distinct Cl limits the scenarios by which the Moon can be built. Here we explore some of those scenarios.

4.1.1. Model 1) heterogeneous loss and fractionation pre- or syn-giant impact

One possibility is that the event responsible for the fractionation of Cl occurred during the giant impact event, perhaps when the material that would eventually re-accrete into the Moon was highly fragmented and at a high temperature (e.g. Canup, 2004). However, this hypothesis—combined with the existence of a low-Cl, low-$\delta^{37}Cl$ reservoir—requires that the Moon contains a second reservoir of chlorine that is isotopically light and low in concentration. A second possibility is that material comprising the Moon was heterogeneously or incompletely degassed, consistent with "shallow" magma ocean hypotheses constrained by the thickness of the lunar crust as observed by GRAIL (Barr, 2016; Wieczorek et al., 2012). However, partial volatile loss is inconsistent with oxygen isotope data on lunar basalts which indicate that the sources of those basalts were well-mixed during the giant impact (Greenwood et al., 2018; Wiechert et al., 2001; Young et al., 2016). It is also unclear whether the temperatures produced by simulations of the giant impact necessarily preclude retention of moderately and highly volatile elements: There are at least three distinct periods during which volatiles could have been lost: 1) the impact and disk phase; 2) the fragmentation

and amalgamation phase; and 3) the magma ocean phase (Boyce et al., 2015; Canup et al., 2015; Elkins-Tanton and Grove, 2011; Hauri et al., 2015; Nakajima and Stevenson, 2018; Pahlevan and Stevenson, 2007). Differentiating between losses occurring during each of these periods is beyond the scope of this paper, but partial/incomplete volatile loss is plausible in all three. Complete volatile loss is only assured in a subset of the models, e.g. those with near-molten, pre-impact protoplanets, or those that predict an accretion timescale for the Moon that is too rapid to permit dissipation of accretionary energy (Barr, 2016). Canup et al. (2015) also propose a model wherein the Moon is composed of material from both the inner (volatile-depleted) disk and outer (relatively volatile-enriched) disk, potentially leading to a heterogeneous Moon with multiple volatile reservoirs. However, it is not clear that this model can generate low-abundance, low-δ^{37}Cl as well as high-abundance, high-δ^{37}Cl reservoirs. So we consider the hypothesis that the Moon was incompletely devolatilized as plausible but not favored.

4.1.2. Model 2) loss and fractionation after the giant impact

A second possibility is that Cl is lost and fractionated after the giant impact, perhaps by late-stage degassing of the lunar magma ocean (Boyce et al., 2015; Dhaliwal et al., 2018). In this hypothesis, early-crystallizing portions of the lunar mantle would incorporate small amounts of unfractionated Cl. Because Cl is not expected to partition into minerals saturating early in the crystallization sequence of the lunar magma ocean, it may be that preservation of Cl in the lunar mantle is accomplished via trapped melt (Hier-Majumder and Hirschmann, 2017). It is also possible that the preservation of unfractionated lunar Cl is reserved for portions of the Moon that never melted, as advocated by "partial magma ocean" models of the formation of the Moon (Shearer et al., 2006, and references therein). Chlorine in the liquid of the magma ocean is eventually partially lost and isotopically fractionated during one or more degassing events before being finally concentrated and trapped as part of the urKREEP (Barnes et al., 2016; Boyce et al., 2015). This is consistent with the presence of two reservoirs, as well as their relative abundances and Cl-isotopic characteristics, but requires that degassing and loss can take place on a planetary scale after the lunar magma ocean has crystallized to a large extent, and potentially with a flotation crust acting as a lid of unknown permeability. Although degassing can take place on some planets at crustal depths and pressures—such as Earth (Parmigiani et al., 2017; Wales and Boyce, 2016)—the general conditions and specific mechanisms that might permit this on the Moon are unknown at this time. Isotopically fractionated material rich in moderately volatile elements such as Zn and Cl has been observed in the "rusty rock" lunar melt breccia 66095 (Day et al., 2017; Sharp et al., 2010a; Shearer et al., 2014). The isotopic signatures of Zn (δ^{66}Zn $= -13.7$‰) and Cl (δ^{37}Cl $= +15$‰) in this rock are consistent with its formation as a condensate of gas that escaped from the crystallizing magma ocean. That this sample formed at or near the surface suggests that volatile elements could escape the magma ocean, again making Model 2 a plausible scenario to explain the observed δ^{37}Cl systematics.

4.2. Our model in the context of Cl isotope data for other lunar rocks

The model proposed here only purports to explain the origin of elevated δ^{37}Cl in low-Ti basalts (including those low-Ti basalts that are trace element enriched and have been historically named as KREEP basalts). We cannot and do not attempt to explain every rock from the Moon with this model. The degree to which high-Ti basalts conform to this or a similar mixing model is poorly constrained, as we lack Cl-isotopic data from trace-element enriched high-Ti basalts at present. More data is also required for highland lithologies, especially those that are apatite-free. Extreme fractionations (δ^{37}Cl $= +67$‰ to $+81$‰) reported by Wang et al. (2012) for lunar meteorite Dhofar 458 may represent additional reservoirs of even more extremely fractionated Cl, or perhaps additional processing of more moderately fractionated Cl by impact melting and degassing (Cohen et al., 2004). Analyses of low-Ti basalts made in the future are predicted to fall on the mixing trends proposed here. However, we also note that many, and possibly all, of the low-Ti mare basalt samples in the present study are derived from the Procellarum KREEP Terrain (PKT), so this model may be limited to low-Ti basalts from this region on the Moon, as hypothesized by Barnes et al. (2016). Future sample return missions that collect low-Ti basalts from outside the PKT may provide a test of this hypothesis. Furthermore, there is no reason to assume that all low-Ti basaltic meteorites are/will be from the PKT, and any from outside that region might confirm this hypothesis if they are found to derive their Cl from a different source with different δ^{37}Cl-trace element systematics.

4.3. Comparison with other volatile element isotope systems

There are few studies comparing isotopic variations for multiple moderately volatile elements in lunar samples: Kato and Moynier (2017) found a correlation between Ga and Zn isotopes, and attributed the fractionations to volatile loss. Day and Moynier (2014) presented a comparison of K, Zn, S, and Cl isotope data sorted by rock type showing similar signs and magnitudes of fractionation for all four isotopes. This could be interpreted as indicating that the timing and mechanism of generation of all four sets of isotope anomalies are the same, but the lack of all four isotope measurements on the same samples indicates that additional work is needed to support those conclusions. Regardless of the origin of the isotope anomalies, the geochemical behavior of these elements could lead to them being decoupled if they were subjected to any petrologic processing after fractionation: Cl and K are highly incompatible, and we would predict that the urKREEP would be a reservoir of isotopically heavy K, as it is of isotopically heavy Cl. This hypothesis is testable, given the recent analytical developments of Wang and Jacobsen (2016b), and we recommend that highly KREEP-enriched low-Ti basalts be the focus of a future lunar K isotope study. What little data exists for Zn partitioning between melt and minerals that might have crystallized from the lunar magma ocean indicates a partitioning value near unity (Davis et al., 2013), consistent with the lack of correlation between Zn abundance and both MgO/(MgO+FeO) and KREEP indicators. If Zn was fractionated early in the history of the Moon along with K and Cl, then (at least portions of) the lunar mantle would be the primary reservoir of heavy Zn, consistent with the conclusions of Kato et al. (2015). However, given that δ^{66}Zn values greater than $+3$‰ have been reported for Mg-suite rocks (Kato et al., 2015), it is also possible that degassing and fractionation happened during the late stages of lunar magma ocean crystallization. In that scenario, the lunar mantle would be a relatively Zn-rich reservoir, whereas the urKREEP would be Zn-poor, but what Zn was present in the urkREEP would be highly fractionated. Coupled δ^{37}Cl–δ^{66}Zn measurements would allow these models to be distinguished and would yield information about the timing of volatile loss in the Moon.

4.4. Abundance of Cl in the bulk silicate Moon

From the modeling presented above we can derive an enrichment factor for Cl, with $Cl_{urKREEP}/Cl_{mare} \sim 28$. In order to determine the bulk Cl content of the silicate portion of the Moon, a robust estimate of the abundance of Cl in a theoretical KREEP-free mare basalt is required, as the urKREEP Cl abundance is a simple multiple of that value. The concentration of Cl in KREEP-free

mare basalt can also be used in conjunction with simple melting models—along with additional, independent constraints—to determine the Cl content of the mare basalt source. These can be combined with rough estimates of the Cl abundances of the volumetrically less significant lunar crust to determine the Cl abundance for the bulk silicate Moon. The bulk Cl content of the Moon can then be used to constrain the extent and mechanisms of volatile loss for the Moon.

4.4.1. The chlorine content of the lunar mantle

McCubbin et al. (2015a) provide a range of Cl abundances for the lunar mantle, from 260 ppb to 2.9 ppm, with the values favored by the authors between 260–320 ppb. Because of its relative size (as much as 588 times the size of the urKREEP; Warren and Wasson, 1979), this value has considerable leverage over the Cl content of the bulk silicate Moon. We chose the lower range of values (260–320 ppb Cl) for our models of the Moon, because they are the most conservative choice in trying to establish the Cl content of the Moon.

4.4.2. The chlorine content of the mare basalt end member

The abundance of Cl in uncontaminated low-Ti mare basalt is critical to determining the bulk Cl content of the Moon because our modeling only constrains the urKREEP Cl content relative to that of hypothetical uncontaminated low-Ti mare basalts. If the lunar mantle has 260–320 ppb Cl, and mare basalts are generated by no more than 30% melting of said mantle (Hauri et al., 2011), then mare basalts should have no less than 900 ppb Cl, assuming that all relevant partition coefficients are zero, again a conservative assumption. This is similar to the lowest Cl abundance observed in olivine-hosted melt inclusions in glass beads (1.14 ppm; Hauri et al., 2011) and by the range of estimated parental melt Cl abundances for low-Ti mare basalts (900 ppb to 6 ppm; McCubbin et al., 2015a), estimated from apatite and bulk rock F abundances from the methods of McCubbin et al. (2015b). Therefore, our preferred range of Cl content for the mare basalt end member is 1–6 ppm.

4.4.3. The chlorine content of the urKREEP and crust

The abundance of Cl in the urKREEP is constrained by modeling Cl isotopes to be approximately 28 times that of uncontaminated mare basalt. Given that uncontaminated mare basalt appears to have 1–6 ppm Cl, we suggest values of 25–170 ppm Cl for the urKREEP, a range that includes previous estimates (Warren, 1989). Recent work by Clay et al. (2017) revises the Cl content of CI chondrite downward from previous estimates (Lodders et al., 2009) by a factor of ~6 to 115 ppm Cl. Using this new, lower value, we constrain the urKREEP to contain between 22–146% of the Cl of CI chondrite. Chlorine (at 0.22–1.5 times CI chondrite) is 50–3400 times less enriched (relative to C.I. chondrite) than the most highly incompatible elements such as U (744 times CI) and Th (759 times CI) as defined by Warren (1989). This is consistent with extensive but incomplete loss of Cl prior to or during the crystallization of the magma ocean.

Adding KREEPy chlorine to the Cl abundance of the mantle, and assuming that the urKREEP:mantle volume ratio is 1:588 increases the bulk silicate Moon Cl estimate from 260 ppb to 0.3–0.6 ppm Cl, meaning that 14–47% of the Moon's Cl is in the urKREEP. This urKREEP/mantle volume ratio—as proposed by Warren and Wasson (1979)—is a maximum, and smaller ratios give higher bulk Cl contents: A model that considers the urKREEP to be 1% of the lunar mantle would produce bulk Cl = 0.5–2 ppm, with ~49–84% of that total Cl coming from the urKREEP.

The Cl content of the lunar crust apart from urKREEP is probably the most difficult component to constrain. Haskin and Warren (1991) report seven bulk Cl analyses ranging from ~0.5–150 ppm Cl, with a mean of 50 ppm. This is much greater than the value we propose for the lunar mantle above (0.4 ppm Cl). Because the crust is volumetrically small (3.6–5.1% of the volume of the bulk silicate Moon), the crust exerts proportionally less leverage on the bulk Cl content of the Moon as compared to the mantle. Nevertheless, if we were to make the irrigorous assertion that the seven bulk analyses are a statistically significant representation of the lunar crust (separate from the urKREEP which is often included in discussions of the crust), inclusion of a 34–43 km thick crust (Wieczorek et al., 2012) with 50 ppm Cl increases our estimates of the bulk silicate Moon abundance to 2–3 ppm Cl. In addition to the obvious caveat that seven analyses are certainly not representative of the bulk lunar crust, it is not clear to what extent the Cl found in crustal rocks is igneous Cl, native to the rock, and to what extent it may in some cases represent metasomatic Cl emplaced in the originally more Cl-poor lithology (Day et al., 2017; Shearer et al., 2014; Treiman et al., 2014). If metasomatic Cl is present in crustal rocks on the Moon, the most obvious source is the urKREEP. This speculation is consistent with the consistently elevated δ^{37}Cl values measured in highlands rocks and regolith samples (Barnes et al., 2016; Day et al., 2017; Sharp et al., 2010a; Shearer et al., 2014; Treiman et al., 2014). Because the concentration and origin of Cl in the non-urKREEP lunar crust is demonstrably uncertain, we will focus on outcomes based on bulk silicate Moon models that exclude the crust, because they are the more conservative choices.

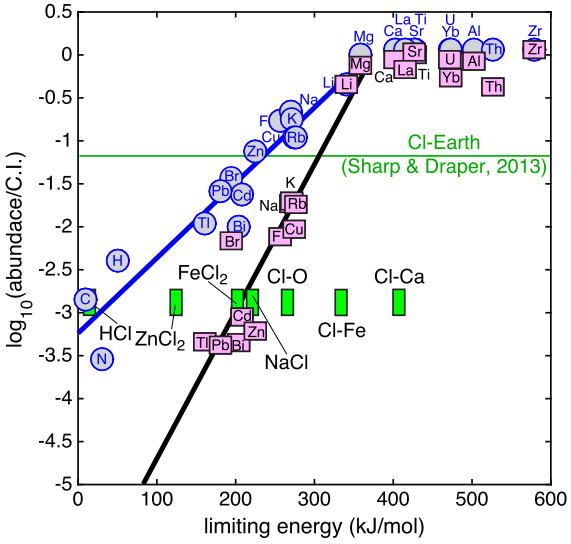

Fig. 4. Model abundances for the Earth (gray circles) and Moon (pink squares) normalized to C.I chondrite, following Albarede et al. (2014), as a function of the energy that limits loss, which is either the bond energy of the element with a logical pair (such as Cl–Ca bonds), or the heat of vaporization of a specific species incorporating the element (such as NaCl). Horizontal green line represents Cl abundance in the bulk silicate Earth calculated from the bulk Earth value reported in Sharp and Draper (2013). Green bars indicate the full range of Cl values compatible with bulk Cl content for the Moon proposed here (for upper and nonzero lower bounds of Cl in the mantle), plotted for various species/bonds that might limit Cl loss. The trend for lunar depletion is consistent with loss being governed by mixtures of more volatile chlorides such as HCl and $ZnCl_2$ with more refractory species such as $FeCl_2$ and NaCl, but inconsistent with loss limited by breaking Cl–Ca or Cl–Fe bonds.

4.4.4. The bulk silicate Moon relative to Earth and CI chondrite

We calculate a range of values from 0.3 to 0.6 ppm Cl for the bulk silicate Moon, a factor of 33–66 lower than the bulk silicate Earth (~20 ppm) determined by Sharp and Draper (2013). This level of Cl retention (1.5–3% of Earth) is consistent with the greater Cl losses expected from the highly isotopically fractionated nature of lunar Cl. These values are considerably higher than many estimates for other elements that we consider to be highly volatile (Fig. 4; Albarede et al., 2014; Lodders, 2003). Such great abundances of Cl appear inconsistent with Cl behaving as

a highly volatile element, as would be expected if the loss of Cl was controlled entirely by the loss of a species such as HCl, which have a high vapor pressure even at low temperatures. However, the position of any element on a plot like Fig. 4 is a function of not only the abundance but also the limiting energy (bond energy or heat of vaporization) chosen (Albarede et al., 2014; Lodders, 2003). In many cases it is reasonable to choose the bond energy with oxygen (X–O), silicon (X–Si), or another element that is abundant in the magmas. It may be that the loss of Cl is limited by breaking Cl–Ca or Cl–Fe bonds: If liberating a Cl- ion from the magma involves breaking a bond between Cl and some other element in the melt, then the energy required can be quite large. Ca–Cl bonds have an energy of 409 kJ/mol, meaning that Cl would behave as a refractory element (Luo and Kerr, 2012). However, it is also possible that those bonds do not limit loss of Cl, perhaps because they are transient in a high-temperature melt at dynamic equilibrium. An alternative is that the loss of a volatile species from the magma is limited by the enthalpy of vaporization of the species that are lost (Albarede et al., 2014). But for an element like chlorine, there are several potentially valid choices with very different limiting energies: If Cl is lost from the magma as HCl, then the limiting energy that must be overcome is the heat of vaporization of HCl (16 kJ/mol; Haynes, 2016), making Cl a highly volatile element. However, if Cl is lost as a more refractory chloride such as NaCl (223 kJ/mol), then the behavior of Cl would be more similar to moderately volatile elements such as Zn and Cd. Loss in a magma is likely controlled by a combination of species, the relative proportion of which is a function of the thermodynamics and geometry of evaporation and transport, a calculation that is beyond the scope of this paper. However, assuming that we have identified all the relevant species, and that the sum of their losses is responsible for the total loss of Cl that we observe, we can place some constraints on the vapor species present at the time of the Cl loss from the Moon that generated the urKREEP reservoir. If the calculated bulk Moon abundances of Cl (for scenarios resulting in the upper and lower bounds of Cl in the mantle as described above) are projected onto the trend of lunar depletion in Fig. 4, then we would expect an average limiting energy of ~200–220 kJ/mol, which are greater than the heat of vaporization of HCl (16 kJ/mol) and $ZnCl_2$ (126 kJ/mol), but similar to those of $FeCl_2$ (204 kJ/mol) and NaCl (223 kJ/mol), and less than any of the bond energies involving the loss of Cl (Luo and Kerr, 2012). The extent of loss of Cl can be explained by a wide range of combinations of more volatile chlorides (HCl, $ZnCl_2$) with more refractory chlorides (NaCl, $FeCl_2$).

4.5. Isotope fractionation associated with Cl loss

Using the relative abundance of Cl in the urKREEP as compared to the mare basalt end-member, and the δ^{37}Cl value for each endmember, we can calculate the bulk δ^{37}Cl of the Moon to be −1.8‰, with values as high as +5.4‰ permissible, depending on the choice of δ^{37}Cl for the mantle (−3‰ or 0‰) and the mantle/urKREEP volume ratio (588 or 100).

Combinations of the above-mentioned species (HCl, NaCl, $FeCl_2$, ZnCl) can also be evaluated relative to the observed isotopic fractionation of Cl for the Moon, which we can calculate from the depletion factor (f) relative to refractory incompatibles such as U and Th, as well as an isotopic signature related to that depletion (δ). For the upper and lower bounds of Cl abundance ($f_{LB} = 0.22/750 = 2.9e{-}4$; $f_{UB} = 1.5/750 = 1.9e{-}3$) relating to $\delta = 25‰$ (from 0‰ to +25‰) we calculate the following fractionation factors: For the lower bound, we find that $\alpha = 0.997$ (or equivalently, $1000 \bullet \ln[\alpha] = -3.04$). For the upper bound, we find that $\alpha = 0.996$ ($1000 \bullet \ln[\alpha] = -3.96$). These $1000 \bullet \ln[\alpha]$ values are smaller than those calculated for NaCl ($\alpha = 0.983$, $1000 \bullet \ln[\alpha] = -17.15$), $FeCl_2$ ($\alpha = 0.992$, $1000 \bullet \ln[\alpha] = -8.03$), and $ZnCl_2$ ($\alpha = 0.993$, $1000 \bullet \ln[\alpha] = -7.02$), but similar to those measured for evaporation of HCl: $\alpha = 0.996$, $1000 \bullet \ln[\alpha] = -3.92$ (Sharp et al., 2010b). Experimental determination of the isotopic fractionation factor for loss of each species from silicate melts under the appropriate conditions will aid in refining which species are involved in the loss of Cl from the Moon. Given that degassing of Cl in the presence of H is thought to be dominated by HCl, constraining the role of HCl loss might also provide independent limits on the abundance of H in the Moon early in its history.

5. Conclusion

Chlorine isotope measurements of the low-Ti basalt suite can be interpreted as representing mixing between two reservoirs: The first is uncontaminated mare basalt, which is low in Cl abundance and also has a low δ^{37}Cl signature (within error of zero per mille). The second is the urKREEP, which is enriched in Cl over the mare basalt model end-member by a factor of ~30, and has distinctively different δ^{37}Cl (~25‰). The bulk Moon δ^{37}Cl value is poorly constrained to also be within error of zero, in stark contrast to the vast majority of measurements made on lunar materials. The presence of multiple ancient reservoirs with different Cl abundances and isotope ratios demands that the processes of building the Moon was capable of generating or preserving a heterogeneous interior. This can be accomplished by incomplete degassing during the giant impact and accretion. In that case KREEP-free mare basalt would represent melts of portions of the Moon that were not degassed during their incorporation into the Moon. Alternatively, the mare basalt end member could represent the early crystallization products of the lunar magma ocean, which preserve less-fractionated—but somewhat degassed—Cl. As the magma ocean was distilled into the urKREEP, degassing took place which resulted in the fractionation of Cl isotopes in the residual liquid. Fractional crystallization-driven distillation of the magma ocean eventually results in the generation of a Cl-rich, high-δ^{37}Cl reservoir (the urKREEP). This model is consistent with the overall depletion of Cl relative to Earth, a value that is in large part driven by the depletion of the mare basalt source mantle.

Models of the formation of the Earth–Moon system are constrained by a number of different kinds of geophysical and geochemical observations (Barr, 2016; Hauri et al., 2015). Provided with the appropriate experimental data to constrain elemental loss and isotopic fractionation at magmatic temperatures and low pressures, it should be possible to use the Cl content of the urKREEP, combined with the calculated depletion factor and the isotope signature of that depletion, to eliminate models of the formation of the Moon that do not result in a body with the correct abundance of Cl and bulk δ^{37}Cl. Additional refinement would be possible using models that account for the crystallization of the lunar magma ocean: such models would be expected to reproduce the heterogeneous distribution of δ^{37}Cl values we predict here (~0‰ in the mantle, +25‰ in the urKREEP). Combined with similar exercises with other moderately volatile isotopic systems such as Zn, Rb, Ga, and K, Cl may prove valuable in the effort to determine how the Moon formed.

Acknowledgements

The authors wish to thank James Day and an anonymous reviewer for their constructive criticism, as well as the reviewing and editorial efforts of Frédéric Moynier, all of which are greatly appreciated. This work was supported by NASA grants to J. Boyce, A. Treiman, and F. McCubbin, with additional support from NASA's Planetary Science Division. J.J. Barnes' contribution was supported by an appointment to the NASA Postdoctoral Program at NASA

Johnson Space Center, administered by Universities Space Research Association under contract with NASA. This work would not have been possible without the pioneering work of Paul Warren, Clive Neal, Francis Albarede, and Zach Sharp.

Appendix A. Supplementary material

Supplementary material related to this article can be found online at https://doi.org/10.1016/j.epsl.2018.07.042.

References

Albarede, F., Albalat, E., Lee, C.-T.A., 2014. An intrinsic volatility scale relevant to the Earth and Moon and the status of water in the Moon. Meteorit. Planet. Sci. 50, 568–577.

Barnes, J., McCubbin, F., Boyce, J., Nguyen, A., Messenger, S., 2017. Volatiles in high titanium basalts from the Moon. In: 48th Lunar and Planetary Science Conference, p. 1727.

Barnes, J.D., Sharp, Z.D., Fischer, T.P., 2008. Chlorine isotope variations across the Izu–Bonin–Mariana arc. Geology 36, 883–886.

Barnes, J.J., Franchi, I.A., McCubbin, F.M., Anand, M., 2018. Multiple volatile reservoirs in the lunar interior revealed by the isotopic composition of chlorine in lunar basalts. Geochim. Cosmochim. Acta, submitted for publication.

Barnes, J.J., Tartèse, R., Anand, M., McCubbin, F.M., Neal, C.R., Franchi, I.A., 2016. Early degassing of lunar urKREEP by crust-breaching impact(s). Earth Planet. Sci. Lett. 447, 84–94.

Barr, A.C., 2016. On the origin of Earth's Moon. J. Geophys. Res., Planets 121, 1573–1601.

Beghein, C., 2010. Radial anisotropy and prior petrological constraints: a comparative study. J. Geophys. Res., Solid Earth 115 (B03303), 1–17.

Boyce, J.W., Liu, Y., Rossman, G.R., Guan, Y., Eiler, J.M., Stolper, E.M., Taylor, L.A., 2010. Lunar apatite with terrestrial volatile abundances. Nature 466, 466–469.

Boyce, J.W., Treiman, A.H., Guan, Y., Ma, C., Eiler, J.M., Gross, J., Greenwood, J.P., Stolper, E.M., 2015. The chlorine isotope fingerprint of the lunar magma ocean. Sci. Adv. 1 (8), 1–8.

Canup, R.M., 2004. Simulations of a late lunar-forming impact. Icarus 168, 433–456.

Canup, R.M., Visscher, C., Salmon, J., Fegley Jr., B., 2015. Lunar volatile depletion due to incomplete accretion within an impact-generated disk. Nat. Geosci. 8, 918–921.

Clay, P.L., Burgess, R., Busemann, H., Ruzié-Hamilton, L., Joachim, B., Day, J.M.D., Ballentine, C.J., 2017. Halogens in chondritic meteorites and terrestrial accretion. Nature 551, 614.

Cohen, B.A., James, O.B., Taylor, L.A., Nazarov, M.A., Barsukova, L.D., 2004. Lunar highland meteorite Dhofar 026 and Apollo sample 15418: two strongly shocked, partially melted, granulitic breccias. Meteorit. Planet. Sci. 39, 1419–1447.

Davis, F.A., Humayun, M., Hirschmann, M.M., Cooper, R.S., 2013. Experimentally determined mineral/melt partitioning of first-row transition elements (FRTE) during partial melting of peridotite at 3 GPa. Geochim. Cosmochim. Acta 104, 232–260.

Day, J.M.D., Moynier, F., 2014. Evaporative fractionation of volatile stable isotopes and their bearing on the origin of the Moon. Philos. Trans. R. Soc. Lond. A 372.

Day, J.M.D., Moynier, F., Shearer, C.K., 2017. Late-stage magmatic outgassing from a volatile-depleted Moon. Proc. Natl. Acad. Sci. USA 114, 9547–9551.

Dhaliwal, J.K., Day, J.M.D., Moynier, F., 2018. Volatile element loss during planetary magma ocean phases. Icarus 300, 249–260.

Elkins-Tanton, L., Grove, T., 2011. Water (hydrogen) in the lunar mantle: results from petrology and magma ocean modeling. Earth Planet. Sci. Lett. 307, 173–179.

Greenwood, J.P., Itoh, S., Sakamoto, N., Warren, P.H., Taylor, L., Yurimoto, H., 2011. Hydrogen isotope ratios in lunar rocks indicate delivery of cometary water to the Moon. Nat. Geosci. 4, 79–82.

Greenwood, R.C., Barrat, J.-A., Miller, M.F., Anand, M., Dauphas, N., Franchi, I.A., Sillard, P., Starkey, N.A., 2018. Oxygen isotopic evidence for accretion of Earth's water before a high-energy Moon-forming giant impact. Sci. Adv. 4, eaao5928.

Hallis, L., Anand, M., Strekopytov, S., 2014. Trace-element modelling of mare basalt parental melts: implications for a heterogeneous lunar mantle. Geochim. Cosmochim. Acta 134, 289–316.

Haskin, L., Warren, P., 1991. Lunar chemistry. In: Lunar Sourcebook, vol. 4, pp. 357–474.

Hauri, E.H., Saal, A.E., Rutherford, M.J., Van Orman, J.A., 2015. Water in the Moon's interior: truth and consequences. Earth Planet. Sci. Lett. 409, 252–264.

Hauri, E.H., Weinreich, T., Saal, A.E., Rutherford, M.C., Van Orman, J.A., 2011. High pre-eruptive water contents preserved in lunar melt inclusions. Science 333, 213–215.

Haynes, W.M., 2016. CRC Handbook of Chemistry and Physics. Taylor & Francis.

Herzog, G., Moynier, F., Albarède, F., Berezhnoy, A., 2009. Isotopic and elemental abundances of copper and zinc in lunar samples, Zagami, Pele's hairs, and a terrestrial basalt. Geochim. Cosmochim. Acta 73, 5884–5904.

Hier-Majumder, S., Hirschmann, M.M., 2017. The origin of volatiles in the earth's mantle. Geochem. Geophys. Geosyst. 18, 3078–3092.

Jerde, E.A., Snyder, G.A., Taylor, L.A., 1993. On the composition of neuKREEP: QMD contamination at Apollo 11? In: Twenty-fourth Lunar and Planetary Science Conference, pp. 719–720.

Jerde, E.A., Taylor, L.A., 1993. Searching for neuKREEP: an EMP study of Apollo 11 Group A basalts. In: Twenty-fourth Lunar and Planetary Science Conference, pp. 717–718.

Joy, K.H., Crawford, I.A., Anand, M., Greenwood, R.C., Franchi, I.A., Russell, S.S., 2008. The petrology and geochemistry of Miller Range 05035: a new lunar gabbroic meteorite. Geochim. Cosmochim. Acta 72, 3822–3844.

Kato, C., Moynier, F., 2017. Gallium isotopic evidence for extensive volatile loss from the Moon during its formation. Sci. Adv. 3, e1700571.

Kato, C., Moynier, F., Valdes, M.C., Dhaliwal, J.K., Day, J.M.D., 2015. Extensive volatile loss during formation and differentiation of the Moon. Nat. Commun. 6, 7617.

Krawczynski, M.J., Grove, T.L., 2012. Experimental investigation of the influence of oxygen fugacity on the source depths for high titanium lunar ultramafic magmas. Geochim. Cosmochim. Acta 79, 1–19.

Liu, Y., Floss, C., Day, J.M.D., Hill, E., Taylor, L.A., 2009. Petrogenesis of lunar mare basalt meteorite Miller Range 05035. Meteorit. Planet. Sci. 44, 261–284.

Lodders, K., 2003. Solar system abundances and condensation temperatures of the elements. Astrophys. J. 591, 1220.

Lodders, K., Palme, H., Gail, H.-P., 2009. 4.4 Abundances of the elements in the solar system. In: Solar System. Springer, pp. 712–770.

Longhi, J., 1992. Experimental petrology and petrogenesis of mare volcanics. Geochim. Cosmochim. Acta 56, 2235–2251.

Luo, Y.-r., Kerr, J., 2012. Bond dissociation energies. In: CRC Handbook of Chemistry and Physics, vol. 89.

McCubbin, F.M., Hauri, E.H., Elardo, S.M., Vander Kaaden, K.E., Wang, J., Shearer Jr., C.K., 2012. Hydrous melting of the martian mantle produced both depleted and enriched shergotites. Geology 40, 683–686.

McCubbin, F.M., Steele, A., Hauri, E.H., Nekvasil, H., Yamashita, S., Hemley, R.J., 2010. Nominally hydrous magmatism on the Moon. Proc. Natl. Acad. Sci. USA 107, 11223–11228.

McCubbin, F.M., Vander Kaaden, K.E., Tartèse, R., Boyce, J.W., Mikhail, S., Whitson, E.S., Bell, A.S., Anand, M., Franchi, I.A., Wang, J., Hauri, E.H., 2015b. Experimental investigation of F, Cl, and OH partitioning between apatite and Fe-rich basaltic melt at 1.0–1.2 GPa and 950–1000 °C. Am. Mineral. 100, 1790–1802.

McCubbin, F.M., Vander Kaaden, K.E., Tartèse, R., Klima, R.L., Liu, Y., Mortimer, J., Barnes, J.J., Shearer, C.K., Treiman, A.H., Lawrence, D.J., 2015a. Magmatic volatiles (H, C, N, F, S, Cl) in the lunar mantle, crust, and regolith: abundances, distributions, processes, and reservoirs. Am. Mineral. 100, 1668–1707.

Meyer, C., 2009. Lunar Sample Compendium. NASA.

Nakajima, M., Stevenson, D.J., 2018. Inefficient volatile loss from the Moon-forming disk: reconciling the giant impact hypothesis and a wet Moon. Earth Planet. Sci. Lett. 487, 117–126.

Neal, C.R., Taylor, L.A., 1989. Metasomatic products of the lunar magma ocean: the role of KREEP dissemination. Geochim. Cosmochim. Acta 53, 529–541.

Pahlevan, K., Stevenson, D.J., 2007. Equilibration in the aftermath of the lunar-forming giant impact. Earth Planet. Sci. Lett. 262, 438–449.

Paniello, R.C., Day, J.M.D., Moynier, F., 2012. Zinc isotope evidence for the origin of the Moon. Nature 490, 376–379.

Parmigiani, A., Degruyter, W., Leclaire, S., Huber, C., Bachmann, O., 2017. The mechanics of shallow magma reservoir outgassing. Geochem. Geophys. Geosyst. 18, 2887–2905.

Potts, N.J., Barnes, J.J., Tartèse, R., Franchi, I.A., Anand, M., 2018. Chlorine isotopic compositions of apatite in Apollo 14 rocks: evidence for widespread vapor-phase metasomatism on the lunar nearside ∼4 billion years ago. Geochim. Cosmochim. Acta 230, 46–59.

Pringle, E.A., Moynier, F., 2017. Rubidium isotopic composition of the Earth, meteorites, and the Moon: evidence for the origin of volatile loss during planetary accretion. Earth Planet. Sci. Lett. 473, 62–70.

Sharp, Z., Draper, D., 2013. The chlorine abundance of Earth: implications for a habitable planet. Earth Planet. Sci. Lett. 369, 71–77.

Sharp, Z.D., Barnes, J.D., Fischer, T.P., Halick, M., 2010b. An experimental determination of chlorine isotope fractionation in acid systems and applications to volcanic fumaroles. Geochim. Cosmochim. Acta 74, 264–273.

Sharp, Z.D., Shearer, C.K., McKeegan, K.D., Barnes, J.D., Wang, Y.Q., 2010a. The chlorine isotope composition of the Moon and implications for an anhydrous mantle. Science 329, 1050–1053.

Shearer, C., Sharp, Z., Burger, P., McCubbin, F., Provencio, P., Brearley, A., Steele, A., 2014. Chlorine distribution and its isotopic composition in "rusty rock" 66095. Implications for volatile element enrichments of "rusty rock" and lunar soils, origin of "rusty" alteration, and volatile element behavior on the Moon. Geochim. Cosmochim. Acta 139, 411–433.

Shearer, C.K., Elardo, S.M., Petro, N.E., Borg, L.E., McCubbin, F.M., 2015. Origin of the lunar highlands Mg-suite: an integrated petrology, geochemistry, chronology, and remote sensing perspective. Am. Mineral. 100, 294–325.

Shearer, C.K., Hess, P.C., Wieczorek, M.A., Pritchard, M.E., Parmentier, E.M., Borg, L.E., Longhi, J., Elkins-Tanton, L.T., Neal, C.R., Antonenko, I., 2006. Thermal and magmatic evolution of the Moon. Rev. Mineral. Geochem. 60, 365–518.

Treiman, A.H., Boyce, J.W., Gross, J., Guan, Y., Eiler, J.M., Stolper, E., 2014. Phosphate–halogen metasomatism of lunar granulite 79215: impact-induced fractionation of volatiles and incompatible elements. Am. Mineral. 99, 1860–1870.

Wales, E., Boyce, J.W., 2016. A terrestrial perspective on the record of lunar volatiles as recorded by apatite. In: 47th Lunar and Planetary Science Conference.

Wang, K., Jacobsen, S.B., 2016a. Potassium isotopic evidence for a high-energy giant impact origin of the Moon. Nature 538, 487–490.

Wang, K., Jacobsen, S.B., 2016b. An estimate of the Bulk Silicate Earth potassium isotopic composition based on MC-ICPMS measurements of basalts. Geochim. Cosmochim. Acta 178, 223–232.

Wang, Y., Guan, Y., Hsu, W., Eiler, J.M., 2012. Water content, chlorine and hydrogen isotope compositions of lunar apatite. In: 75th Annual Meteoritical Society Meeting. Abs. #5170.

Warren, P., 1989. KREEP: major-element diversity, trace-element uniformity (almost). In: Workshop on Moon in Transition: Apollo 14, KREEP, and Evolved Lunar Rocks, pp. 149–153.

Warren, P.H., Wasson, J.T., 1978. The last dregs of the lunar magma. Lunar Planet. Sci. 9, 1231–1233.

Warren, P.H., Wasson, J.T., 1979. The origin of KREEP. Rev. Geophys. Space Phys. 17, 73–88.

Wiechert, U., Halliday, A., Lee, D.-C., Snyder, G., Taylor, L., Rumble, D., 2001. Oxygen isotopes and the Moon-forming giant impact. Science 294, 345–348.

Wieczorek, M.A., Neumann, G.A., Nimmo, F., Kiefer, W.S., Taylor, G.J., Melosh, H.J., Phillips, R.J., Solomon, S.C., Andrews-Hanna, J.C., Asmar, S.W., 2012. The crust of the Moon as seen by GRAIL. Science, 1231530.

Xing, Z., Beghein, C., 2015. A Bayesian approach to assess the importance of crustal corrections in global anisotropic surface wave tomography. Geophys. Suppl. Mon. Not. R. Astron. Soc. 203, 1832–1846.

Young, E.D., Kohl, I.E., Warren, P.H., Rubie, D.C., Jacobson, S.A., Morbidelli, A., 2016. Oxygen isotopic evidence for vigorous mixing during the Moon-forming giant impact. Science 351, 493–496.